Comparison of Backbone and Tryptophan Side-Chain Dynamics of Reduced and Oxidized *Escherichia coli* Thioredoxin Using ^{15}N NMR Relaxation Measurements†

Martin J. Stone,‡ Kasibhatla Chandrasekhar,‡,§ Arne Holmgren,‖ Peter E. Wright,*,‡ and H. Jane Dyson*,‡

Department of Molecular Biology, The Scripps Research Institute, La Jolla, California 92037, and Department of Biochemistry, The Medical Nobel Institute, Karolinska Institutet, Box 60400, S-10401 Stockholm, Sweden

Received September 15, 1992; Revised Manuscript Received October 27, 1992

ABSTRACT: The backbone and tryptophan side-chain dynamics of both the reduced and oxidized forms of uniformly ^{15}N-labeled *Escherichia coli* thioredoxin have been characterized using inverse-detected two-dimensional ^1H-^{15}N NMR spectroscopy. Longitudinal (T_1) and transverse (T_2) ^{15}N relaxation time constants and steady-state {^1H}-^{15}N NOEs were measured for more than 90% of the protonated backbone nitrogen atoms and for the protonated indole nitrogen atoms of the two tryptophan residues. These data were analyzed by using a model free dynamics formalism to determine the generalized order parameter (S^2), the effective correlation time for internal motions (τ_e), and ^{15}N exchange broadening contributions (R_{ex}) for each residue, as well as the overall molecular rotational correlation time (τ_m). The reduced and oxidized forms exhibit almost identical dynamic behavior on the picosecond to nanosecond time scale. The W31 side chain is significantly more mobile than the W28 side chain, consistent with the positions of W31 on the protein surface and W28 buried in the hydrophobic core. Backbone regions which are significantly more mobile than the average include the N-terminus, which is constrained in the crystal structure of oxidized thioredoxin by specific contacts with a Cu^{2+} ion, the C-terminus, residues 20–22, which constitute a linker region between the first α-helix and the second β-strand, and residues 73–75 and 93–94, which are located adjacent to the active site. In contrast, on the microsecond to millisecond time scale, reduced thioredoxin exhibits considerable dynamic mobility in the residue 73–75 region, while oxidized thioredoxin exhibits no significant mobility in this region. The possible functional implications of the dynamics results are discussed.

Thioredoxin is a ubiquitous, multifunctional protein, with the conserved active site residues Cys-Gly-Pro-Cys forming a disulfide bridge in the oxidized form (thioredoxin-S_2)[1] (Holmgren, 1985; Gleason & Holmgren, 1988). Thioredoxin-S_2 is reduced by NADPH and the flavoprotein thioredoxin reductase to form thioredoxin-$(SH)_2$, which contains two thiol groups (Holmgren, 1985). Thioredoxin-$(SH)_2$ is a powerful protein disulfide reductase, and thioredoxin catalyzes dithiol–disulfide exchange reactions (Holmgren, 1985).

In addition to the role of thioredoxin as a redox catalyst, *Escherichia coli* thioredoxin-$(SH)_2$ is required as a subunit to induce the DNA polymerase and exonuclease activities of the phage T7 gene 5 protein in *E. coli* cells infected with bacteriophage T7 (Modrich & Richardson, 1976; Adler & Modrich, 1983; Huber et al., 1986) and to support filamentous phage assembly (Russel & Model, 1985, 1986). Thioredoxin-S_2 is unable to promote these activities, but mutant thioredoxins containing Cys to Ser or Cys to Ala mutations at one or both of the active site cysteine residues retain partial activity, indicating that the requirement for the reduced rather than the oxidized form resides, at least in part, in a structural rather than a chemical difference between the two forms (Huber et al., 1986). Detailed characterization of the structure and dynamics of both oxidation states of thioredoxin is required in order to understand the activity differences.

E. coli thioredoxin is an 11.7-kDa protein containing 108 amino acids. The structure of a Cu^{2+} complex of the oxidized form has been solved and refined to 1.7-Å resolution (Holmgren & Söderberg, 1970; Holmgren et al., 1975; Katti et al., 1990); the crystals used in this study contained two molecules of thioredoxin-S_2 per asymmetric unit, and local structural differences resulting from crystal contacts were observed between the two molecules. No crystals have been obtained for the reduced form. Complete ^1H and ^{15}N NMR resonance assignments have been obtained for both the reduced and oxidized forms in solution (Dyson et al., 1989; Chandrasekhar et al., 1991), and the solution structure of thioredoxin-$(SH)_2$ has been calculated from NMR distance restraints (Dyson et al., 1990). Reduced thioredoxin and oxidized thioredoxin have identical secondary structures and tertiary folds, consisting of a five-stranded twisted β-sheet surrounded by three α-helices and one 3_{10} or irregular helix. The active site cysteine residues are located on a turn between the second β-strand and the second α-helix, and the loop residues 75–76 and 91–93 are close to the active site and, together with active site residues 33 and 34, form a hydrophobic surface (Eklund et al., 1984). Structural differences between the reduced and oxidized forms are extremely subtle and are

† This work was supported by Grants GM 36643 (P.E.W.) and GM 43238 (H.J.D.) from the National Institutes of Health and Grant 13X-3529 from the Swedish Medical Research Council and P. A. Hedlunds Stiftelse (A.H.).

* To whom correspondence should be addressed.

‡ The Scripps Research Institute.

§ Present address: Department of Biological Chemistry and Molecular Pharmacology, Harvard Medical School, 240 Longwood Ave., Boston, MA 02115.

‖ Karolinska Institutet.

[1] Abbreviations: thioredoxin-S_2, oxidized *Escherichia coli* thioredoxin; thioredoxin-$(SH)_2$, reduced *E. coli* thioredoxin; NADPH, reduced nicotinamide adenine dinucleotide phosphate; NMR, nuclear magnetic resonance; T_1, longitudinal relaxation time constant; T_2, transverse relaxation time constant; $T_{2\rho}$, transverse relaxation time constant in the rotating frame; NOE, nuclear Overhauser effect; CSA, chemical shift anisotropy; CPMG, Carr–Purcell–Meiboom–Gill; FID, free induction decay; rms, root mean square.

0006-2960/93/0432-426$04.00/0

limited to the immediate vicinity of the active site, as evidenced by chemical shift differences in this region (Dyson et al., 1988) [the conclusion that the χ^1 angle of C35 differs by 122° between the two oxidation states (Dyson et al., 1990) was based on an erroneous assignment of an NOE (Dyson et al., unpublished results)]. While these minor differences between the crystal structure of the oxidized form and the average solution structure of the reduced form could contribute to the observed activity differences, an alternative possibility is that changes in dynamics accompanying the oxidation state change allow the reduced form access to structural states which are unavailable to the oxidized form. In order to investigate this possibility, we have undertaken a detailed study of the backbone dynamics of both reduced and oxidized thioredoxin based on ^{15}N NMR relaxation measurements.

The measurement of ^{15}N and ^{13}C NMR relaxation rates provides information about the internal dynamics of proteins on time scales faster than the rotational correlation time. The primary mechanism of relaxation for these nuclei is the dipolar interaction with the directly bound protons; chemical shift anisotropy (CSA) provides a secondary relaxation mechanism at high magnetic field strengths (Abragam, 1961; London, 1980). Recently, a number of reports have appeared in which ^1H-detected two-dimensional heteronuclear NMR experiments have been used to characterize ^{15}N or ^{13}C relaxation in proteins (Nirmala & Wagner, 1988; Kay et al., 1989; 1992; Clore et al., 1990a; Palmer et al., 1991a; Schneider et al., 1992; Stone et al., 1992; Kördel et al., 1992; Nicholson et al., 1992; Barbato et al., 1992). Generally, the experimental results have been analyzed using the model free formalism of Lipari and Szabo (1982a,b), in which the motions are described by the overall rotational correlation time, τ_m, a generalized order parameter, S^2, and an effective internal correlation time, τ_e. In particular cases, extensions to this formalism may be warranted (Clore et al., 1990a,b; Fedotov & Kivayeva, 1987; Zang et al., 1990).

EXPERIMENTAL PROCEDURES

Sample Preparation. Uniformly labeled recombinant thioredoxin was obtained as described previously (Chandrasekhar et al., 1991). Samples were prepared for NMR spectroscopy by solvent exchange on a Sephadex G25 column. Reduced thioredoxin was obtained by the addition of dithiothreitol to a solution of oxidized thioredoxin (Dyson et al., 1989; Chandrasekhar et al., 1991).

NMR Measurements. The ^{15}N T_1 and T_2 relaxation time constants and $\{^1H\}$-^{15}N NOEs were measured from ^{15}N-^1H correlation spectra, recorded using the sensitivity-enhanced ^1H-detected pulse sequences described by Kördel et al. (1992). The interval between the refocusing pulses in the ^{15}N Carr–Purcell–Meiboom–Gill (CPMG; Carr & Purcell, 1954; Meiboom & Gill, 1958) sequence of the T_2 experiment was 1.0 ms, which is sufficiently short to effectively spin–lock the heteronuclear spins (Vold & Vold, 1976; Palmer et al., 1992). In the T_1 and T_2 experiments, the spectra obtained from each orthogonal magnetization component were added together to yield a single spectrum with a sensitivity enhancement of $\sqrt{2}$ relative to a conventional spectrum recorded in the same time (Palmer et al., 1991b). In the NOE experiment, each orthogonal component was used to obtain an independent measurement of the NOE; thus, performing the experiment twice afforded four independent measurements of the NOE, required for the NOE uncertainties to be estimated.

All NMR spectra were recorded at 308 K on a Bruker AMX500 spectrometer, equipped with a three-channel interface. For the T_2 experiments, an auxiliary amplifier (Model 3205, American Microwave Technology) was used to generate high-power ^{15}N pulses at the repetition rate necessitated by the CPMG sequence. The duty cycle during the ^{15}N CPMG sequence was <10% in order to minimize contributions from sample heating and $T_{2\rho}$. A total of 4K complex points were acquired in ω_2, with a spectral width of 12.5 kHz, and the ^1H carrier was placed on the H_2O signal; 400 increments were collected in ω_1 with a spectral width of 2.04 kHz and with the ^{15}N carrier at 120.5 ppm. Solvent suppression in all experiments was achieved by the use of spin–lock purge pulses (Messerle et al., 1989) and postacquisition application of a low-pass filter to the time domain data (Marion et al., 1989).

For measurements of T_1 and T_2 rate constants, a recycle delay of 1.7 s was used between acquisitions to ensure sufficient recovery of ^1H magnetization. For measurements of the $\{^1H\}$-^{15}N NOE, a recycle delay of 5.0 s, approximately five times the longest ^{15}N T_1, was used between scans to ensure that maximal NOEs developed before acquisition. The T_1 and T_2 experiments were repeated using several different values of the delay T (used to denote the longitudinal relaxation period in the T_1 experiment or the duration of the CPMG sequence in the T_2 experiment). For T_1 measurements seven T delays were used [37, 123, 242, 500, 1014, 2026, and 3037 ms for thioredoxin-$(SH)_2$ and 36, 121, 238, 491, 996, 1988, and 2981 ms for thioredoxin-S_2], while for T_2 measurements eight T delays were used [4, 42, 100, 200, 350, 500, 800, and 1200 ms for thioredoxin-$(SH)_2$ and 4, 42, 80, 200, 350, 500, 800, and 1200 ms for thioredoxin-S_2].

Data Analysis. Spectra were processed on Sparc SLC or Iris Indigo computers using modified versions of the FTNMR software package (Hare Research). Each spectrum was processed twice in order to evaluate separately well-resolved and moderately overlapped cross peaks. In the first instance 4-Hz line broadening was applied in ω_2; in the second instance a Lorentzian–Gaussian transformation was used. In both instances a cosine bell followed by a Lorentzian–Gaussian transformation was used in ω_1. These weighting functions were selected to minimize the uncertainties in the measured peak heights while avoiding any systematic errors arising from cross-peak overlap or FID truncation artifacts. A simple spline baseline correction routine was employed in ω_2.

Relaxation rate constants and NOE enhancements were calculated from cross-peak heights in the ^1H–^{15}N correlation spectra. Data analysis was performed on a Convex C240 computer with programs written in FORTRAN 77; commercial (IMSL, Houston, TX) and published (Press et al., 1986) numerical algorithms were used as applicable. The uncertainties in the measured peak heights were estimated by repeating the experiments at the shortest and longest time points for T_1 measurements and at four time points [T = 4, 80 or 100, 200, and 800 ms] for T_2 measurements. Differences between peak heights in the duplicate spectra were evaluated for a representative set of cross peaks, and the standard deviation of the differences were divided by $\sqrt{2}$ to yield the uncertainty in the peak heights themselves (Palmer et al., 1991a). Uncertainties for those time points not duplicated were estimated by interpolation of the uncertainties for the duplicated points.

The longitudinal relaxation times, T_1, were obtained by a three-parameter nonlinear least-squares fit of the equation

$$I(T) = I_\infty - [I_\infty - I_0] \exp(-T/T_1) \quad (1)$$

to the experimental data, while the transverse relaxation times, T_2, were obtained by two- or three-parameter nonlinear fits, respectively, of the equations

$$I(T) = I_0 \exp(-T/T_2) \quad (2)$$

or

$$I(T) = I_\infty + I_0 \exp(-T/T_2) \quad (3)$$

In eq 1–3, I_0 and I_∞ are the initial and final cross-peak heights, respectively. Curve fitting used the Levenburg–Marquardt algorithm (Press et al., 1986) to minimize the value of a χ^2 goodness-of-fit parameter, as described previously (Palmer et al., 1991a; Stone et al., 1992). Uncertainties in the relaxation rates were taken to be the standard errors of the fitted parameters. The sufficiencies of the monoexponential decay functions given by eq 1–3 were evaluated with a χ^2 test, as described by Palmer et al. (1991a). For the T_2 data, the significance of the improvement afforded by the three-parameter model (eq 3) over the two-parameter model (eq 2) was evaluated using an F statistic (Ratkowsky, 1983; Wright et al., 1988; Stone et al., 1992).

The steady-state NOEs were calculated as the ratios of peak heights in the spectrum recorded with proton saturation to those in the spectrum recorded without saturation; the average values of the NOEs and standard errors in the mean were determined from the four separate data sets.

As described in detail elsewhere (Kay et al., 1989; Clore et al., 1990a; Stone et al., 1992), the relaxation of protonated ^{15}N nuclei is dominated by dipolar and chemical shift anisotropy (CSA) interactions with the attached protons, which in turn are dependent on the values of the spectral density function $J(\omega)$ at five characteristic frequencies; in specific cases, a contribution to the ^{15}N transverse relaxation rate ($1/T_2$) due to conformational exchange (R_{ex}) may also be significant (Clore et al., 1990a; Stone et al., 1992). Since there was insufficient experimental relaxation data to determine uniquely these five values of the spectral density function, $J(\omega)$ was approximated by using the model free formalism of Lipari and Szabo (1982a,b)

$$J(\omega) = (2/5)\left[\frac{S^2\tau_m}{1 + (\omega\tau_m)^2} + \frac{(1 - S^2)\tau}{1 + (\omega\tau)^2}\right] \quad (4)$$

in which S^2 is the generalized order parameter, which measures the degree of spatial restriction of the unit bond vector, and $1/\tau = 1/\tau_m + 1/\tau_e$, where τ_m is the overall rotational correlation time of the molecule and τ_e is the effective correlation time describing internal motions. In this model, the overall tumbling of the molecule is assumed to be isotropic; the principal components of the inertial tensor of thioredoxin-S_2 are calculated from the crystal structure to be in the approximate ratio 1.00:1.16:1.37, indicating that the overall motion is unlikely to be significantly anisotropic. The value of S^2 ranges from 0, generally taken to indicate isotropic internal motions (although specific anisotropic motional models can yield $S^2 = 0$; Lipari & Szabo, 1982a), to 1 for internal motion that is completely restricted relative to a fixed molecular frame of reference. If all internal motions are very fast ($\tau_e < 10$ ps), the spectral density function (eq 4) may be simplified to

$$J(\omega) = (2/5)S^2\tau_m/[1 + (\omega\tau_m)^2] \quad (5)$$

Calculation of the model free parameters from the measured relaxation rate constants and the NOE enhancements was performed by minimization of the target function

$$\chi^2 = \sum_{i=1}^{r}\Gamma_i = \sum_{i=1}^{r}[(R_{1i} - R_{1i}^*)^2/\sigma_{1i}^2 + (R_{2i} - R_{2i}^*)^2/\sigma_{2i}^2 + (NOE_i - NOE_i^*)^2/\sigma_{NOEi}^2] \quad (6)$$

in which Γ_i is the sum of the squared residuals; R_{1i}, R_{2i}, and NOE_i are the experimental values of the relaxation parameters ($R_1 = 1/T_1$ and $R_2 = 1/T_2$); σ_{1i}, σ_{2i}, and σ_{NOE_i} are the uncertainties in the rate constants and NOEs; and R_{1i}^*, R_{2i}^*, and NOE_i^* are the values of the relaxation parameters back-calculated from the model free dynamics parameters for the ith ^{15}N nucleus. The summation extends over the r nuclei included in the calculation. Procedures used to find the optimum values and uncertainties of the model free parameters based on the measured relaxation rate constants and NOE enhancements were identical to those described by Palmer et al. (1991a); the difference between parallel and perpendicular components of the chemical shift tensor was taken to be –160 ppm for backbone amide NH groups (Hiyama et al., 1988; Shoji et al., 1989) and –89 ppm for tryptophan side-chain indole NH groups (Cross & Opella, 1983).

RESULTS

Resolved Peaks. The ^1H and ^{15}N resonances of the backbone NH groups and the two tryptophan side-chain NH groups in thioredoxin have been assigned previously (Dyson et al., 1989; Chandrasekhar et al., 1991). In the present work, 98 cross peaks for thioredoxin-$(SH)_2$ and 95 cross peaks for thioredoxin-S_2 were sufficiently well resolved for peak heights to be measured accurately in the T_1, T_2, and NOE experiments; these included the side-chain NH groups of W28 and W31 in both forms. The backbone resonances of D9 and F102 could be quantitated in the T_2 and NOE experiments with thioredoxin-S_2 but were not identified in the T_1 experiment.

As in earlier studies (Palmer et al., 1991a; Stone et al., 1992; Kördel et al., 1992), peak heights rather than volumes were used to characterize the intensities of resonances in the heteronuclear correlation spectra. Uncertainties in the peak heights for T_1 and T_2 measurements were estimated by recording duplicate spectra. The variances in the peak heights were close to the variances in the baseplane noise levels for the later time points; however, for the earlier time points the peak height uncertainties exceeded the root mean square (rms) noise levels by factors of 1.7–8. As observed previously (Stone et al., 1992), both peak height uncertainties and rms noise levels decreased at later time points in the inversion–recovery and CPMG experiments, possibly as a result of improved solvent suppression at longer time points.

T_1 Values. The peak heights of several resonances in each form of thioredoxin are plotted against time T in Figure 1 and fitted by nonlinear regression to a three-parameter exponential decay (eq 1). The χ^2 test indicated that the curve fits were adequate statistically and that the peak height uncertainties had been estimated realistically. The decay constants, T_1, and uncertainties, for backbone resonances, are plotted versus residue number in panels A and B of Figure 2 for oxidized and reduced thioredoxin, respectively. The average uncertainties in the measured T_1 values are 2.4% for oxidized and 1.0% for reduced thioredoxin. The data show similar trends for both oxidized and reduced forms. For most residues, the T_1 values lie in the range 0.4–0.5 s. While there are no T_1 values significantly lower than 0.4 s, residues with T_1 values conspicuously higher than 0.5 s include G21, A22, R73, G74, A93, L94, and A108. In addition, the two residues closest to

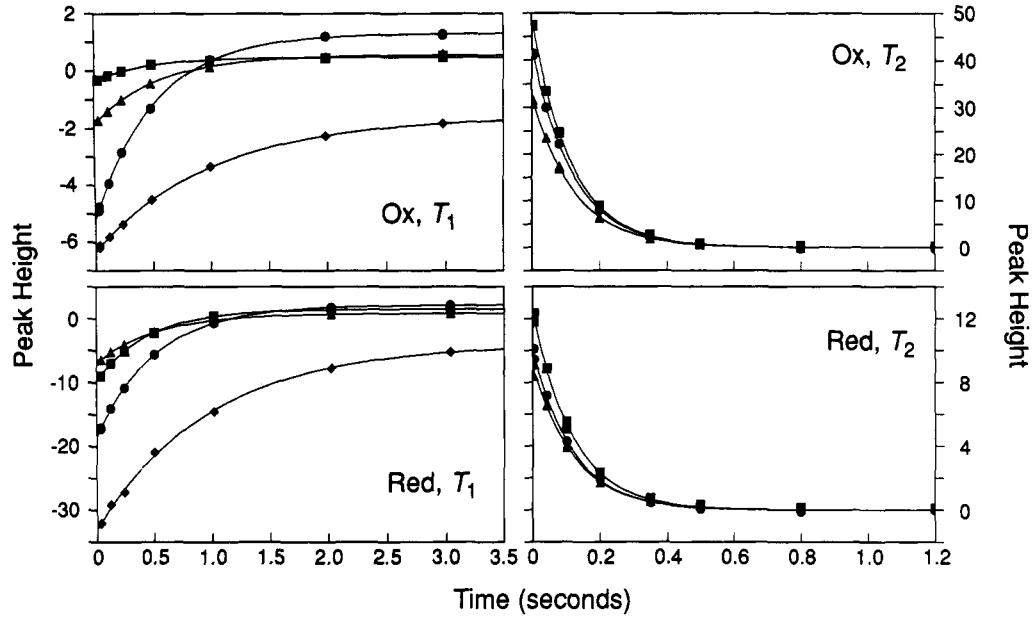

FIGURE 1: T_1 relaxation curves (left panels) for oxidized (Ox) and reduced (Red) thioredoxin, fit to eq 1, for T14 (●), C32 (■), R73 (▲), and A108 (♦). T_2 relaxation curves (right panels) for oxidized and reduced thioredoxin for H6 (●), Y49 (■), and G65 (▲), fit to eq 2 or 3, selected according to the criteria discussed in the text; Y49 and G65 in reduced thioredoxin are fit to eq 3, while all other T_2 curves are fit to eq 2. Peak heights are shown on arbitrary absolute scales, and the uncertainties in the peak heights are less than 0.05 and 0.06 unit for the T_1 measurements of oxidized and reduced thioredoxin, respectively, and less than 0.9 and 0.5 unit for the T_2 measurements of oxidized and reduced thioredoxin, respectively.

the N-terminus whose amide resonances have been identified, K3 and I4, both have T_1 values slightly higher than 0.5 s.

T_2 Values. Curve fits were performed for two-parameter and three-parameter exponential functions (eq 2 and 3, respectively); examples of the fits are shown in Figure 1. Three-parameter fits were used for all residues for which the F statistic exceeded the 95% critical F value, while two-parameter fits were used for all other residues (Stone et al., 1992). Using this criterion, T_2 relaxation data were selected to be fitted by the two-parameter function for 90 resonances of thioredoxin-S_2 and 69 resonances of thioredoxin-$(SH)_2$. In the remaining cases, where the three-parameter function was used, the fitted final cross-peak height (I_∞, eq 3) was never more than 3% of the initial cross-peak height (I_0). The χ^2 values indicated adequate statistical fits and well-estimated peak height uncertainties. The T_2 values and uncertainties are plotted in panels C and D of Figure 2; the average uncertainties are 1.0% and 1.6% for oxidized and reduced thioredoxin, respectively. As observed for the T_1 data, the T_2 data show the same trends for both the oxidized and reduced forms. Most residues have T_2 values in the range 0.10–0.13 s. However, a number of residues exhibit slower relaxation; these include K3, I4, D20, G21, A22, G74, L94, and A108.

NOE Values. The NOE of each residue was determined for each data set as the ratio of the peak height in the spectrum recorded with proton saturation to that in the spectrum recorded without proton saturation. The average NOEs and uncertainties, determined from four independent NOE measurements resulting from two sensitivity-enhanced experiments, are plotted in panels E and F of Figure 2. The average uncertainties are 1.5% for thioredoxin-S_2 and 2.8% for thioredoxin-$(SH)_2$. Once again, oxidized thioredoxin and reduced thioredoxin exhibit very similar trends. For most residues the NOEs lie in the range 0.70–0.80. The NOEs of residues G21 and A108 are negative, while those of K3, I4, D20, A22, R73, G74, A93, and L94 are all significantly less than 0.70.

As has been discussed previously, if the T_1 of the water is sufficiently long and chemical exchange or spin diffusion between the amide protons and the water is sufficiently fast, the measured NOE may be artificially decreased as a result of incomplete equilibration of the amide ^{15}N and ^1H magnetization during the experiment acquired without proton saturation (Jelinski et al., 1980; Smith et al., 1987; Kay et al., 1989; Clore et al., 1990a; Stone et al., 1992). In studies of other proteins, these errors have generally been sufficiently small to be ignored (Clore et al., 1990a; Stone et al., 1992; Kördel et al., 1992). In the present work, the water T_1 was measured to be 4.3 s in both samples studied, and the relevant relaxation delay was 5.0 s; these are similar values to those used in earlier studies. Furthermore, order parameters calculated using only the T_1 and T_2 data were qualitatively and in most cases quantitatively the same as those calculated using all three relaxation parameters. Thus, the NOE data were considered to be unaffected by exchange or spin diffusion errors.

Tryptophan Side-Chain NH Groups. The relaxation data for the side-chain indole NH groups of W28 and W31 were analyzed in a manner identical to that of the backbone amide groups; the T_1, T_2, and NOE values are listed in Table I. The parameters for the W28 side-chain NH group are in the normal range for backbone NH groups. However, the T_1 value of the W31 side-chain NH is considerably higher than the normal backbone range in both thioredoxin-S_2 and thioredoxin-$(SH)_2$, and the T_2 value is below the normal backbone range in thioredoxin-S_2 and close to the lower limit in thioredoxin-$(SH)_2$. The relaxation data were included in the model free analyses described below using a chemical shift anisotropy of −89 ppm (Cross & Opella, 1983).

Initial Estimation of τ_m. Under conditions where $\tau_e < 100$ ps, $\tau_m > 1$ ns, and T_2 is not shortened significantly by chemical exchange, the ratio T_1/T_2 is essentially independent of S^2 and τ_e and provides an initial estimate of the overall molecular correlation time τ_m (Kay et al., 1989; Clore et al., 1990a). Using the average T_1/T_2 ratio, τ_m was estimated to be 6.57 ns for thioredoxin-S_2 and 6.54 ns for thioredoxin-$(SH)_2$.

Model Free Analyses. Criteria are required to determine whether an effective internal correlation time, τ_e (eq 4) and/

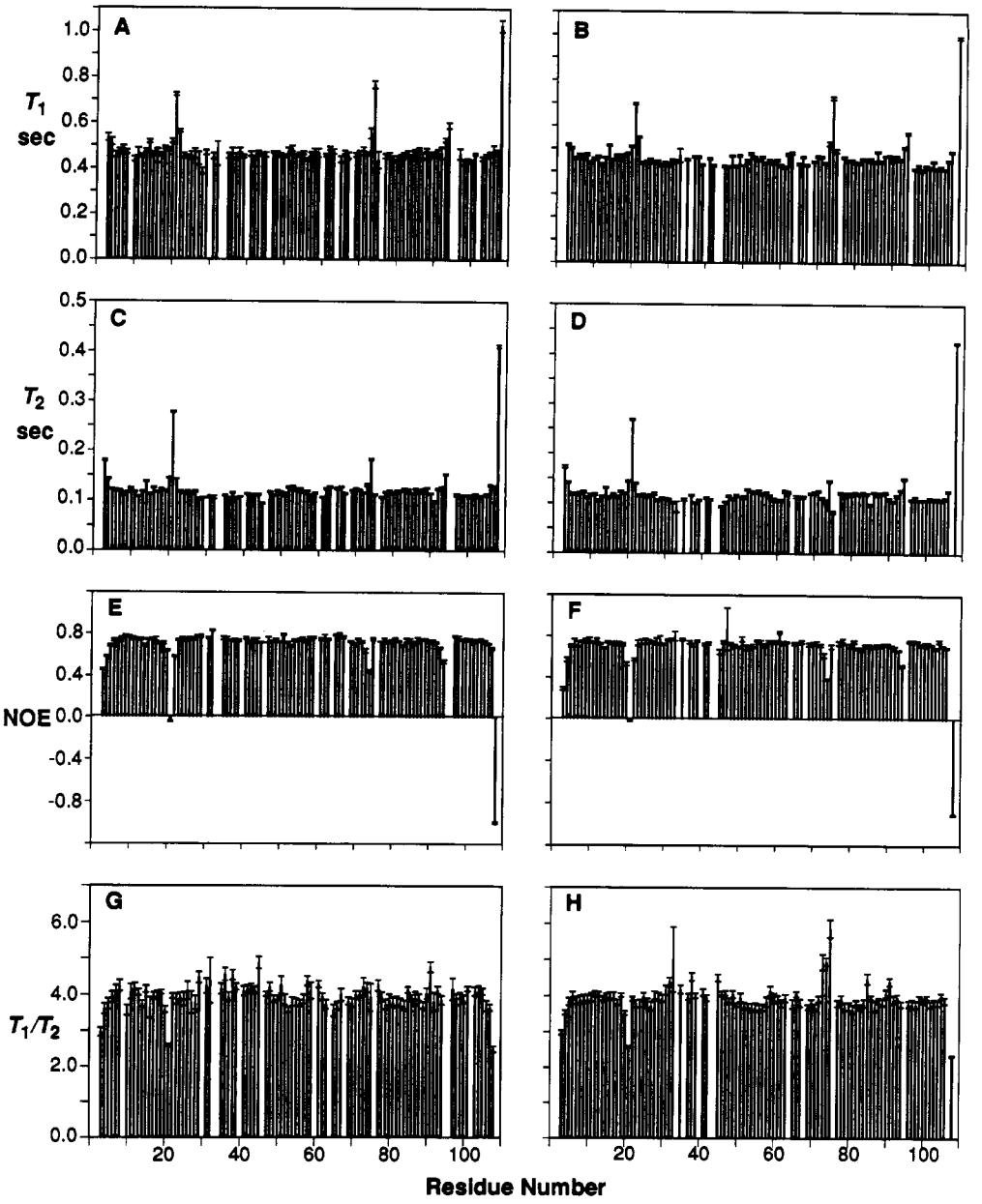

FIGURE 2: Measured relaxation parameters (T_1, T_2, and {^{1}H}–^{15}N NOE) and T_1/T_2 ratios for the resolved backbone NH groups in oxidized and reduced thioredoxin: T_1 values for (A) oxidized and (B) reduced thioredoxin; T_2 values for (C) oxidized and (D) reduced thioredoxin; {^{1}H}–^{15}N NOEs for (E) oxidized and (F) reduced thioredoxin; and T_1/T_2 ratios for (G) oxidized and (H) reduced thioredoxin. T_1 and T_2 data were obtained by fitting the measured peak heights with eq 1–3, as appropriate. NOE values and their uncertainties are the averages and the standard deviations, respectively, of the values determined from each of four data sets.

or a ^{15}N exchange broadening term, R_{ex}, must be incorporated into the model free analysis in order to satisfy the experimental data for each residue; the molecular correlation time τ_m and the order parameter S^2 were always included. Clore et al. (1991a) have used the following criteria: τ_e was included if the T_1/T_2 ratio was more than one sample deviation below the mean, and R_{ex} was included if the T_1/T_2 ratio was more than one sample deviation above the mean. The T_1/T_2 ratios for thioredoxin are plotted in panels G and H of Figure 2 for backbone resonances and listed in Table I for tryptophan side-chain resonances. Applying the above criteria (Clore et al. 1991a) to these data, τ_e would be selected for the backbone resonances of residues 3, 10, 21, 65, and 108 of thioredoxin-S_2 and residues 3, 21, and 108 of thioredoxin-$(SH)_2$, while R_{ex} would be selected for residues 29, 32, 36, 38, 45 and 91 (backbone) and residue 31 (side chain) of thioredoxin-S_2 and residues 32, 33, 38, 45, 73, 74, 75, 85, and 91 (backbone) and residue 31 (side chain) of thioredoxin-$(SH)_2$. An alternative variable selection protocol (Stone et al., 1992) involves a series of Monte Carlo simulations of trial analyses that include the various possible terms and then selection of those variables which are non-zero in the trial analyses. This alternative method was used in the current study because it allows incorporation of both τ_e and R_{ex} terms for a single residue and it can allow identification of residues whose τ_e and/or R_{ex} values are statistically non-zero but which were not selected by the Clore et al. criteria (Stone et al., 1992). Thus, the model free analyses for each form of thioredoxin were performed as follows:

(a) A preliminary calculation was performed in which τ_m was fixed at the estimated value, R_{ex} was held at 0, and S^2 and τ_e (eq 4) were optimized for each resonance. In cases where the optimized value of τ_e was non-zero (within 95% confidence limits), τ_e was optimized in the final calculation. Otherwise, τ_e was assumed to be 0 in the final calculation.

Table I: Relaxation and Dynamics Parameters for Tryptophan Side-Chain NH Groups[a]

parameter	W28		W31	
	oxidized	reduced	oxidized	reduced
T_1 (s)	0.51 ± 0.01	0.501 ± 0.004	0.57 ± 0.01	0.560 ± 0.006
T_2 (s)	0.126 ± 0.002	0.127 ± 0.002	0.093 ± 0.002	0.106 ± 0.002
NOE	0.74 ± 0.02	0.69 ± 0.02	0.71 ± 0.02	0.66 ± 0.02
T_1/T_2	4.1 ± 0.2	3.96 ± 0.09	6.1 ± 0.3	5.3 ± 0.2
S^2_{sc}	0.91 ± 0.04	0.93 ± 0.04	0.82 ± 0.04	0.81 ± 0.04
τ_e (ps)	11.8 ± 0.5	56 ± 3	14.7 ± 0.8	35 ± 2
R_{ex} (Hz)	0.44 ± 0.02	*b*	4.0 ± 0.2	2.8 ± 0.1
S^2_{bb}	1.00 ± 0.04	0.95 ± 0.04	0.95 ± 0.04	0.90 ± 0.04

[a] Shown are the measured relaxation parameters (T_1, T_2, and {^{1}H}–^{15}N NOE), the T_1/T_2 ratio, and the calculated dynamics parameters (S^2_{sc}, τ_e, and R_{ex}) for the side-chain indole NH group of each tryptophan residue in oxidized and reduced thioredoxin. The order parameter S^2_{bb} for each tryptophan backbone NH group is also listed. [b] The R_{ex} term was not selected for optimization for the W28 side-chain NH group in thioredoxin-$(SH)_2$.

Table II: Dynamics Parameters Optimized in Final Model Free Calculations[a]

	oxidized	reduced
no. of resonances in calculation	95	98
neither τ_e nor R_{ex} was optimized for	2	1
τ_e was optimized but R_{ex} was not for	49	62
R_{ex} was optimized but τ_e was not for	4	4
both τ_e and R_{ex} were optimized for	40	31
total no. of input relaxation parameters	285	294
total no. of dynamics parameters optimized	229	227
optimized molecular correlation time, τ_m (ns)	6.41 ± 0.04	6.30 ■ 0.01

[a] Shown is a summary of the input relaxation parameters and optimized dynamics parameters in the final model free calculations for oxidized and reduced thioredoxin; parameters were selected for optimization using the criteria discussed in the text. The optimized values for the overall molecular rotational correlation time, τ_m, are also listed.

(b) A second preliminary calculation was performed in which τ_m was held at the estimated value and τ_e was held at 0, while S^2 (eq 5) and R_{ex} were optimized for each resonance. In cases where the optimized value of R_{ex} was non-zero, R_{ex} was optimized in the final calculation. Otherwise, R_{ex} was assumed to be 0.

(c) A final calculation was performed by optimizing τ_m for the whole molecule, S^2 for each resonance, and τ_e and/or R_{ex} for the resonances selected in (a) and (b) above. The parameters chosen for optimization and the optimized τ_m values are listed in Table II; the optimized S^2, τ_e, and R_{ex} values are plotted in Figure 3 for backbone resonances and listed in Table I for tryptophan side-chain resonances.

The average (±standard deviation) of the order parameters is 0.86 ± 0.01 in the oxidized and 0.87 ± 0.01 in the reduced form of thioredoxin. Resonances which have S^2 values statistically lower than average in both forms are K3, I4, T14, D20, G21, A22, R73, G74, A93, L94, and A108; these residues, and residues 1 and 2, are colored red in the backbone trace of thioredoxin-S_2 shown in Figure 4. There are no resonances whose order parameters are lower than average in only one form although comparative data were unavailable for D9, E30, G33, K36, D43, E44, A46, I60, K96, F102, and L107. Furthermore, the only resonances whose order parameters are statistically different between the two forms are K3, G21, I75, E85, V91, and D104; of these, the S^2 value of I75 differs by 3.2 standard deviations between the two forms (being lower in the reduced form) while for the other five resonances the S^2 values differ by 2.1–2.3 standard deviations.

In order to assess the reliability of the τ_e and R_{ex} data, a series of simulations were performed for a subset of the residues in which the sensitivity of the optimization function, Γ_i (eq 6), to variation of either τ_e or R_{ex} was evaluated (Figure 5). In about half of the cases studied (e.g., D20 and Q50 in thioredoxin-S_2, panel A, Figure 5), the optimization function had a sharp minimum when τ_e was varied, giving confidence in the optimized τ_e values; in the remaining cases (e.g., Q98 and L103 in thioredoxin-S_2, panel A, Figure 5), the curves showed very broad minima, implying that the τ_e values are poorly defined. The curves showing the dependence of the optimization function on variation of R_{ex} (panel B, Figure 5) exhibited well-defined minima, indicating that the R_{ex} values are unlikely to be in error by more than 0.5 Hz, although the uncertainties obtained using Monte Carlo simulations may be underestimated. These simulations also indicated that the optimized values of S^2 were not very sensitive to the values at which τ_e and R_{ex} were fixed as long as these values were chosen within a realistic range (data not shown).

Considering the results of these simulations, the τ_e values (panels C and D of Figure 3) cannot in general be interpreted with confidence; in contrast, confident interpretation of the R_{ex} values (panels E and F of Figure 3) is justified. For most resonances, the R_{ex} values are less than 1.5 Hz. The only resonances with R_{ex} values significantly greater than 1.5 Hz were the side-chain resonances of W31 in both forms, the backbone resonances of I45 in both forms, and G33, I38, R73, G74, and I75 in the reduced form; all of these resonances have significantly higher than average T_1/T_2 ratios.

The sufficiencies of the fits in the model free analyses were evaluated by comparing the experimentally determined relaxation data with relaxation parameters back-calculated from the optimized dynamics parameters. These values generally agreed to within 10%, so incorporation of a second time scale into the model free analysis would not have been justified (Clore et al., 1990a,b).

DISCUSSION

Backbone Dynamics. The order parameters for reduced and oxidized thioredoxin are remarkably similar. For both forms of the protein there are five regions, highlighted in Figure 4, which exhibit higher than average mobility on the picosecond to nanosecond time scale. The C-terminal residue, A108, has the lowest order parameter (0.22), indicating that this residue is highly mobile. Similarly, while the amide resonance of residue D2 has not been observed (itself an indication of mobility and/or rapid exchange), both K3 and I4 have order parameters significantly lower than normal, suggesting that the N-terminus is also highly flexible. Flexibility of the terminal regions is consistent with previous structural studies of thioredoxin. In solution, the first β-strand (β_1) begins at residue 4, according to dihedral angles, but I5 is the first hydrogen-bonded residue (Dyson et al., 1989, 1990); the extension of strand β_1 to residue 2 in the crystal structure of thioredoxin-S_2 is probably due to binding of a Cu^{2+} ion in this region (Katti et al., 1990). Indeed, the absolute requirement of Cu^{2+} for crystallization seems to reflect a need to damp the motions of the disordered N-terminus [attempts to crystallize thioredoxin-$(SH)_2$ under analogous conditions to thioredoxin-S_2 have been unsuccessful since Cu^{2+} oxidizes thioredoxin-$(SH)_2$ (Holmgren, 1985)]. Crystallographic *B* values for the N-terminus of thioredoxin-S_2 are only slightly higher than average. While the amide proton of the C-terminal residue is hydrogen bonded to the carbonyl group of D104 in 11 of the 12 best restrained solution structures of thioredoxin-$(SH)_2$, the medium-range NOEs involving A108 are weaker than would be expected for a regular α-helix, and there is a large

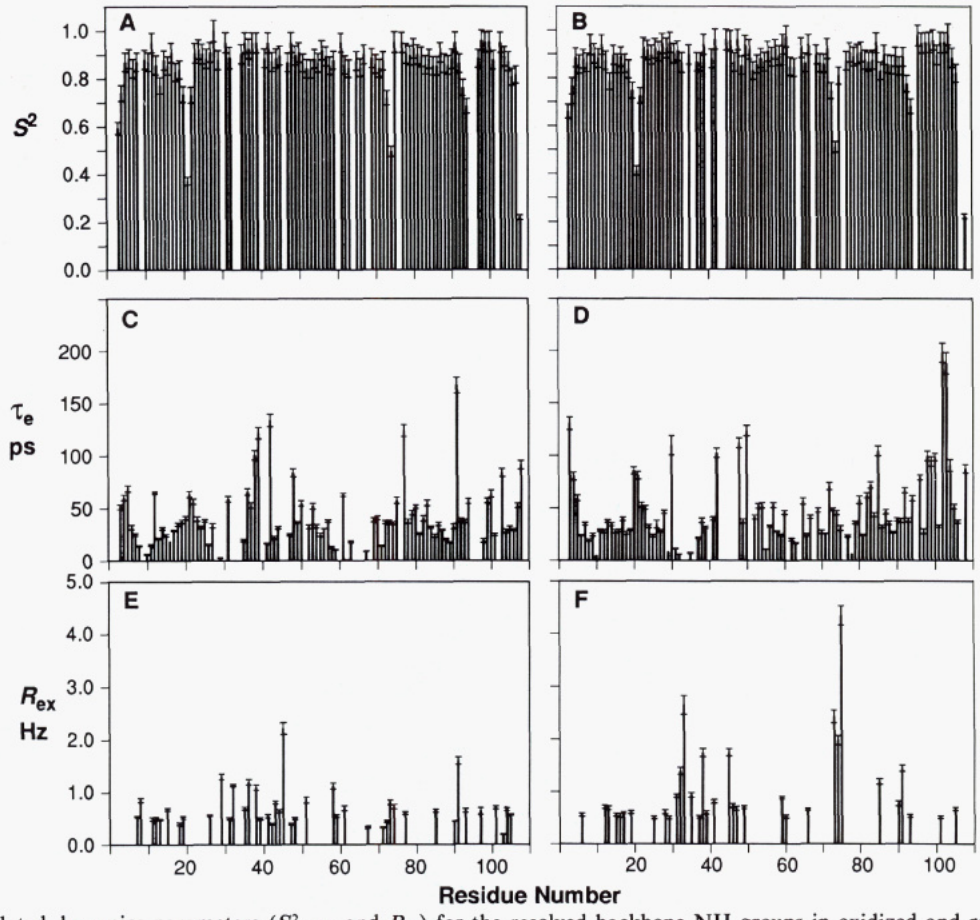

FIGURE 3: Calculated dynamics parameters (S^2, τ_e, and R_{ex}) for the resolved backbone NH groups in oxidized and reduced thioredoxin: generalized order parameters, S^2, for (A) oxidized and (B) reduced thioredoxin; effective internal correlation times, τ_e, for (C) oxidized and (D) reduced thioredoxin; and ^{15}N exchange broadening terms, R_{ex}, for (E) oxidized and (F) reduced thioredoxin. Data were calculated from the relaxation parameters shown in Figure 2 according to the criteria discussed in the text and summarized in Table II.

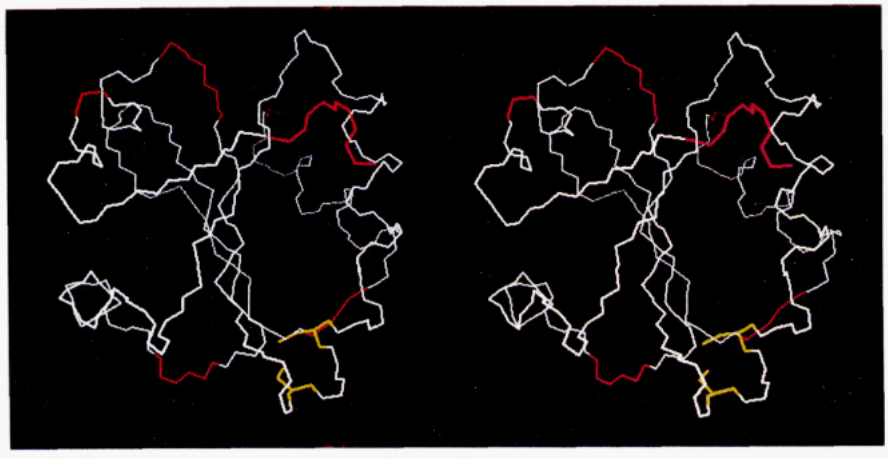

FIGURE 4: Stereoview of the backbone structure of oxidized thioredoxin with the active site cysteine residues (side chains shown) in yellow and the residues with statistically lower than average order parameters in red; also in red are residues 1 and 2 which are assumed to be highly flexible. Residues 1–4 are at the top right; residues 14 and 20–22 are at the top left; residues 73–74 are at the bottom left; residues 93–94 are at the bottom right; and residue 108 is at the top center at the back. Coordinates are those of molecule A in the thioredoxin-S_2 crystal structure (Katti et al., 1990).

backbone deviation between the two molecules of thioredoxin-S_2 in the asymmetric unit of the crystal, suggesting that the backbone is flexible in this region. Low order parameters are commonly observed at the N- and/or C-termini of proteins (Kay et al., 1989; Clore et al., 1990a; Palmer et al., 1991; Schneider et al., 1992; Stone et al., 1992; Kördel et al., 1992).

There are three internal regions where the S^2 values are significantly lower than average for both forms of the protein (Figure 4). The first of these, residues 20–22, is situated between the first α-helix (α_1) and the second β-strand (β_2). In a number of the solution structures of thioredoxin-$(SH)_2$, the peptide groups involving the amide nitrogens of D20, G21, and A22 are involved in backbone–backbone hydrogen bonds (Dyson et al., 1990). However, hydrogen bonds involving both the carbonyl group of G21 and the NH group of A22 are mediated through water molecules in the thioredoxin-S_2 crystal structure, and while there are five reverse turns in thioredoxin-S_2 which conform to one of the six normal classifications (Richardson, 1981), the geometry of the chain reversal at residues 19–22 cannot be classified in this way

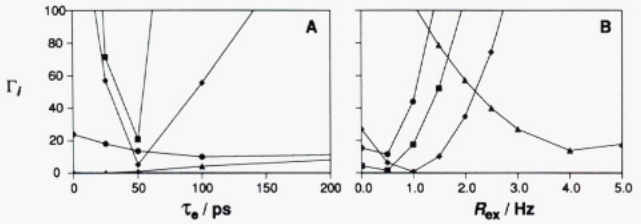

FIGURE 5: Graphs illustrating the sensitivity of the sum of the squared residuals (Γ_i, eq 6) to variation of (A) τ_e for D20 (■), Q50 (♦), Q98 (▲), and L103 (●) in thioredoxin-S_2 and (B) R_{ex} for D10 (■), C35 (♦), I75 (▲), and K100 (●) in thioredoxin-$(SH)_2$. Each point on these curves was obtained by performing a model free calculation in which either τ_e or R_{ex} was fixed at the value indicated on the horizontal axis while the other of these two variables was fixed at zero, τ_m was fixed at the optimized value listed in Table II, and S^2 was varied until the minimum value of Γ_i was obtained.

(Katti et al., 1990). Again, there is a large difference in this region between the two molecules in the asymmetric unit; in particular, the D20 side chain of one molecule forms an intermolecular hydrogen bond to E85 in the other molecule. Considering that this turn is situated on the opposite side of the molecule from the active site, the high mobility is unlikely to be of functional importance. Indeed, in phage T4 thioredoxin (glutaredoxin) the peptide chain starts with the equivalent of the second β-strand in *E. coli* thioredoxin (Söderberg et al., 1978).

The two other internal regions with significant picosecond to nanosecond time-scale mobility are R73–G74 and A93–L94 (Figure 4). Residues R73 and G74 are located between the region of irregular helical structure (residues ca. 64–72) and the fourth β-strand (β_4, residues 77–82) and are exposed to solvent; residues 74–77, including *cis*-Pro76, form a type VIb β-turn. Residues A93 and L94 lie between the last β-strand (residues 88–92) and the C-terminal α-helix (residues 96–108), and L94 has unusual χ^1 and χ^2 angles in the crystal structure of thioredoxin-S_2, allowing the side chain to pack getween I38 and the initial residues in the C-terminal α-helix. Both of these regions are spatially close to the active site, as illustrated in Figure 6; possible functional consequences of the mobility in this region are discussed below.

The only other residue whose order parameter is statistically lower than average (Figure 4) is T14, which occurs in the middle of α_1 (residues 11–18). The NH group of T14 is hydrogen bonded to the carbonyl group of D10 in 10 of the 12 best restrained molecular dynamics structures of thioredoxin-$(SH)_2$ (Dyson et al., 1990), but the helical structure of α_1 in both the crystal and the solution is irregular, with T14 and adjacent residues have unusual ϕ and ψ angles (Katti et al., 1990; Dyson et al., 1990). In one of the two molecules in the crystal asymmetric unit, residues 11–21 lack well-defined density, implying that α_1 is disordered. However, picosecond to nanosecond time-scale fluctuations in solution are localized to residue 14.

While the residues with low order parameters are generally found in loop or terminal regions, not all loop residues have low order parameters. No significant correlations could be identified between order parameters and (a) secondary structure type, (b) participation of the NH group or the associated carbonyl group in hydrogen bonds, (c) amide ^1H or ^{15}N chemical shift differences between thioredoxin-$(SH)_2$ and thioredoxin-S_2, (d) root mean square deviation from the average positions of backbone amide ^1H and/or ^{15}N atoms in the solution structure of thioredoxin-$(SH)_2$, or (e) thioredoxin-S_2 crystallographic *B* factors. The lack of such correlations is generally consistent with studies of other proteins (Kay et al., 1989; Clore et al., 1990a; Schneider et al., 1992; Stone et al., 1992; Kördel et al., 1992), although, in the case of ubiquitin, a dependence of S^2 on participation in hydrogen bonds was proposed (Schneider et al., 1992) and, in the case of calbindin D_{9k}, S^2 values correlated with both crystallographic *B* factors and hydrogen-exchange rates (Kördel et al., 1992); hydrogen-exchange rates have not been measured for thioredoxin. Although the factors which govern the picosecond to nanosecond time-scale mobility of NH groups in proteins remain poorly understood, the consensus of this and earlier studies is that residues which are buried within the hydrophobic core or which occur in the middle of regular secondary structures rarely have S^2 values significantly lower than average, while those which occur in irregular secondary structure, in loops, or on the protein surface often, but not always, have low order parameters.

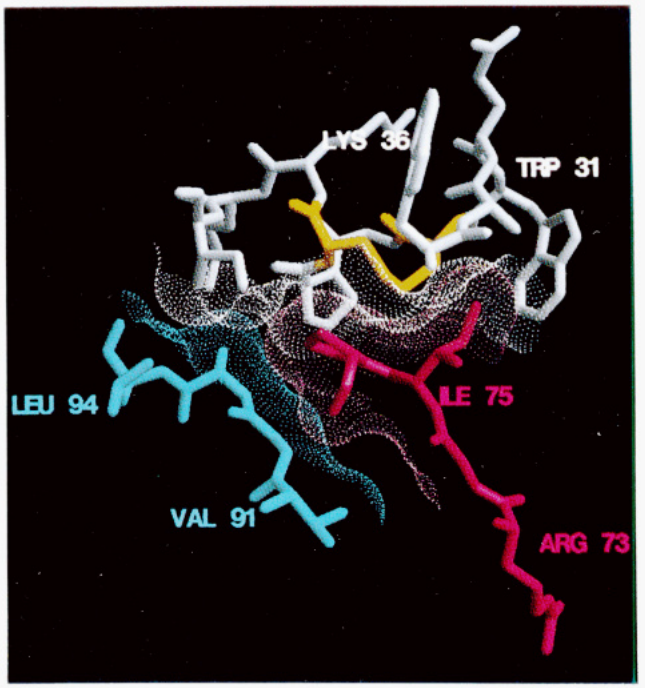

FIGURE 6: View showing the packing of residues adjacent to the active site of molecule A in the thioredoxin-S_2 crystal structure (Katti et al., 1990). Residues 28–38 are shown in white, with the exception of C32 and C35 which are in yellow, residues 73–76 are shown in red, and residues 91–94 are shown in blue. The surfaces of contact between the three regions are illustrated in the same colors as the participating residues; these surfaces were generated using the molecular surface (ms) program (Connolly, 1983). This figure was produced using the graphics program GRAMPS (O'Donnell & Olson, 1981).

In the current study, the only significant dynamic difference identified between the reduced and oxidized forms of thioredoxin is that residues 73, 74, and 75 show considerably higher microsecond to millisecond time-scale mobility in the reduced form, as indicated by the R_{ex} values (panels E and F of Figure 3). Since the only chemical difference between the two oxidation states of thioredoxin occurs in the C32 and C35 side chains, the observed dynamic difference must result from the changes that occur at these active site residues. Although the residue 73–75 region is distant in the peptide sequence from the active site cysteine residues, the side chain of I75 packs directly onto the disulfide bridge in the crystal structure of thioredoxin-S_2, as illustrated in Figure 6 (Katti et al., 1990). It is therefore physically reasonable that breaking the disulfide bond should result in greater mobility of I75. Indeed, this is the only residue with a significant mobility difference between oxidized and reduced states on both picosecond–nanosecond

and microsecond–millisecond time scales. Residues R73 and G74 are not in direct contact with the active site residues (Figure 6). However, the side chain of R73 points into the solvent, and G74 lacks a side chain, so these residues are unrestrained by packing interactions. It appears that the increased microsecond to millisecond time-scale mobility of I75 is propagated through the backbone to the preceding two residues. In contrast, the residues following I75 are *cis*-P76, which is likely to be inherently less flexible than other residues, and T77 and L78, which are constrained within the antiparallel β-sheet. Relaxation parameters were not measured for the proline residues in thioredoxin since they lack amide protons. No significant mobility changes on reduction were observed for residues 77 and 78. We note that the microsecond to millisecond time-scale mobility in this region cannot be associated with cis–trans isomerization of P76 (Langsetmo et al., 1989) which would be expected to occur on a much slower time scale (Grathwohl & Wüthrich, 1981). There are other indications that the active site region of reduced thioredoxin has greater flexibility on this time scale. The R_{ex} value of I38, whose side chain packs between those of C35, P76, and L94 in the crystal structure of thioredoxin-S_2, is slightly larger in thioredoxin-$(SH)_2$. In addition, the R_{ex} value of G33 is high in thioredoxin-$(SH)_2$; relaxation data for G33 in thioredoxin-S_2 were not measurable due to a low signal to noise ratio for this peak. Thus, it appears that several of the residues surrounding the active site are more flexible in the reduced than in the oxidized protein.

The fact that residues 73–75 are far removed in the primary sequence from the active site cysteine residues yet still exhibit flexibility changes on disulfide oxidation–reduction provides dramatic evidence that backbone mobility in proteins may be influenced by the packing of side chains in the tertiary protein structure. It was noted earlier that dynamics is also affected by participation in regular secondary structure.

Tryptophan Side-Chain Mobility. This is the first report of model free dynamics parameters calculated for the side-chain NH groups of tryptophan residues in a protein. Both of the tryptophan residues in thioredoxin are located close to the active site. The side chain of W28 is packed in the hydrophobic core, although the NH group of this side chain is hydrogen bonded to a water molecule in the crystal structure of thioredoxin-S_2. In contrast, the W31 side chain is situated on the protein surface, packed against the C32 and I75 side chains, with its indole NH group hydrogen bonded to the carboxyl group of D61 in the crystal structure (Katti et al., 1990). Consistent with the different structural environments of these side chains, the order parameter of the W31 side-chain NH is significantly lower than that of the W28 side-chain NH (Table I), although both are within the same range as most backbone NH groups. In addition, the microsecond to millisecond time-scale mobility of the W31 side chain, as indicated by R_{ex} values (Table I), is much higher than average, while motion of the W28 side chain is not significant on this time scale. The order parameters for side-chain NH groups are generally slightly lower than those for the backbone NH groups in the same tryptophan residue (Table I), indicating that some side-chain motions may be occurring independently of backbone mobility in these residues.

Comparison with Previous Studies. The dynamics of thioredoxin has been studied by time-resolved tryptophan and tyrosine fluorescence spectroscopy and molecular dynamics simulations (Elofsson et al., 1991). Fluorescence measurements of wild-type and W31F mutant thioredoxin in both reduced and oxidized forms generally yielded molecular rotational correlation times in the range 5–7 ns, consistent with the values obtained in this study, although the tryptophan fluorescence of wild-type thioredoxin-S_2 gave anomalously low values of 2.3 and 3.5 ns for 280- and 300-nm excitation wavelengths, respectively. The latter values were taken as an indication that the motional behavior of the W28 side chain was more complex than the simple assumed model of independent internal and overall motions. In constrast, the current NMR data appear to fit this simple model satisfactorily. In studies of a zinc finger peptide and calbindin D_{9K}, molecular rotational correlation times measured by NMR and fluorescence have been in good agreement (Palmer et al., manuscript in preparation; Kördel et al., 1992).

Using the Stokes–Einstein equation (Dwek, 1973) and values for partial specific volumes reported by Kaminsky and Richards (1992), the rotational correlation times at 308 K are calculated to be 2.60 and 2.46 ns for oxidized and reduced thioredoxin, respectively. These values are considerably lower than the experimentally determined correlation times, as has also been observed for enzyme IIA^{Glc} (Stone, unpublished results) and calbindin D_{9K} (Kördel et al., 1992). In addition, the partial specific volume of thioredoxin-S_2 is 5 ± 1% higher than that of thioredoxin-$(SH)_2$, implying that the τ_m of thioredoxin-S_2 should also be 5 ± 1% higher. The current data indicate that the τ_m of thioredoxin-S_2 is 2–2.5% higher than that of thioredoxin-$(SH)_2$, which is at least qualitatively in accordance with the partial specific volume measurements.

Molecular dynamics simulations of oxidized and reduced thioredoxin (Elofsson et al., 1991) indicate that the W28 side chain is highly motionally restricted on the picosecond time scale in both forms, while the W31 side chain is considerably more mobile. The present data correlate well with these simulations. Slight differences between the tryptophan side-chain mobility in the oxidized and reduced states predicted by the molecular dynamics simulations were not detected in the present study.

Functional Implications of Dynamics. The flexibility of the N- and C-termini of thioredoxin and the residue 20–22 region is unlikely to be of functional importance since these regions are not known to participate in interactions with other proteins. In contrast, the spatial proximity to the active site of mobile residues 73–75 and 93–94 suggests a possible functional role. The structure of thioredoxin in the vicinity of the active site is shown in Figure 6. Eklund et al. (1984) have identified residues 33–34, 75–76, and 91–93 as a flat hydrophobic surface, conserved throughout members of the thioredoxin/glutaredoxin family, adjacent to the active site and implicated in binding to protein substrates. In *E. coli* thioredoxin W31 also contributes to this surface while residues 38, 73, 74, and 94 are immediately adjacent to this hydrophobic region. Although it is not known whether the structure of thioredoxin changes on binding to other proteins, the observed conformational flexibility of the loop residues 73–74 and 93–94 on a picosecond to nanosecond time scale may be important in allowing structural rearrangement or assisting the binding of other proteins at the active site region of thioredoxin; a mobile loop adjacent to the active site has also been identified in enzyme IIA^{Glc} (Stone et al., 1992).

While no significant structural differences have so far been detected between the average solution structure of thioredoxin-$(SH)_2$ and the crystal structure of thioredoxin-S_2, the difference in microsecond to millisecond time-scale dynamics between the two forms of thioredoxin in solution implies that certain structural states are kinetically accessible to thioredoxin-(SH_2) which are not accessible to thioredoxin-S_2. This

could potentially explain the ability of reduced but not oxidized thioredoxin to induce the DNA polymerase and exonuclease activities of the phage T7 gene 5 protein.

ACKNOWLEDGMENT

We thank Dr. Arthur G. Palmer, Dr. Mark Rance, Mikael Akke, and Garry Gippert for helpful discussions, Dr. Arthur G. Palmer for access to data analysis programs and for critical comments on the manuscript, Dr. John Cavanagh for assistance with relaxation experiments, Dr. Arthur Olson for help with molecular graphics, and Linda Tennant for assistance with protein purification and sample preparation.

SUPPLEMENTARY MATERIAL AVAILABLE

Two tables giving the values and uncertainties, for each residue, of the experimentally determined T_1, T_2, and NOE data, the optimized order parameters, and (where applicable) internal correlation times and ^{15}N exchange broadening terms (6 pages). Ordering information is given on any current masthead page.

REFERENCES

Abragam, A. (1961) *Principles of Nuclear Magnetism*, pp 264–353, Clarendon Press, Oxford.
Adler, S., & Modrich, P. (1983) *J. Biol. Chem. 258*, 6956–6962.
Barbato, G., Ikura, M., Kay, L. E., Pastor, R. W., & Bax, A. (1992) *Biochemistry 31*, 5269–5278.
Carr, H. Y., & Purcell, E. M. (1954) *Phys. Rev. 94*, 630–638.
Chandrasekhar, K., Krause, G., Holmgren, A., & Dyson, H. J. (1991) *FEBS Lett. 284*, 178–183.
Clore, G. M., Driscoll, P. C., Wingfield, P. T., & Gronenborn, A. M. (1990a) *Biochemistry 29*, 7387–7401.
Clore, G. M., Szabo, A., Bax, A., Kay, L. E., Driscoll, P. C., & Gronenborn, A. M. (1990b) *J. Am. Chem. Soc. 112*, 4989–4991.
Connolly, M. L. (1983) *Science 221*, 709–713.
Cross, T. A., & Opella, S. J. (1983) *J. Am. Chem. Soc. 105*, 306–308.
Dwek, R. A. (1973) *Nuclear Magnetic Resonance in Biochemistry: Applications to Enzyme Systems*, pp 242–243, Clarendon Press, Oxford.
Dyson, H. J., Holmgren, A., & Wright, P. E. (1988) *FEBS Lett. 228*, 254–258.
Dyson, H. J., Holmgren, A., & Wright, P. E. (1989) *Biochemistry 28*, 7074–7087.
Dyson, H. J., Gippert, G. P., Case, D. A., Holmgren, A., & Wright, P. E. (1990) *Biochemistry 29*, 4129–4136.
Eklund, H., Cambillau, C., Sjöberg, B.-M., Holmgren, A., Jörnvall, H., Höög, J.-O., & Bränden, C.-I. (1984) *EMBO J. 3*, 1443–1449.
Elofsson, A., Rigler, R., Nilsson, L., Roslund, J., Krause, G., & Holmgren, A. (1991) *Biochemistry 30*, 9648–9656.
Fedotov, V. D., & Kivayeva, L. S. (1987) *J. Biomol. Struct. Dyn. 4*, 599–619.
Gleason, F. K., & Holmgren, A. (1988) *FEMS Microbiol. Rev. 54*, 271–298.
Grathwohl, C., & Wüthrich, K. (1981) *Biopolymers 20*, 2623–2633.
Hiyama, Y., Niu, C.-H., Silverton, J. V., Bavoso, A., & Torchia, D. A. (1988) *J. Am. Chem. Soc., 110*, 2378–2383.
Holmgren, A. (1985) *Annu. Rev. Biochem. 54*, 237–271.
Holmgren, A., & Söderberg, B.-O. (1970) *J. Mol. Biol. 54*, 387–390.
Holmgren, A., Söderberg, B.-O., Eklund, H., & Brändén, C.-I. (1975) *Proc. Natl. Acad. Sci. U.S.A. 72*, 2305–2309.
Huber, H. E., Russel, M., Model, P., & Richardson, C. C. (1986) *J. Biol. Chem. 261*, 15006–15012.
Jelinski, L. W., Sullivan, C. E., & Torchia, D. A. (1980) *J. Magn. Reson. 41*, 133–139.
Kaminsky, S. M., & Richards, F. M. (1992) *Protein Sci. 1*, 22–30.
Katti, S., LeMaster, D. M., & Eklund, H. (1990) *J. Mol. Biol. 212*, 167–184.
Kay, L. E., Torchia, D. A., & Bax, A. (1989) *Biochemistry 28*, 8972–8979.
Kay, L. E., Nicholson, L. K., Delaglio, F., Bax, A., & Torchia, D. A. (1992) *J. Magn. Reson. 97*, 359–375.
Kördel, J., Skelton, N. J., Akke, M., Palmer, A. G., III, & Chazin, W. J. (1992) *Biochemistry 31*, 4856–4866.
Langsetmo, K., Fuchs, J., & Woodward, C. (1989) *Biochemistry 28*, 3211–3220.
Lipari, G., & Szabo, A. (1982a) *J. Am. Chem. Soc. 104*, 4546–4559.
Lipari, G., & Szabo, A. (1982b) *J. Am. Chem. Soc. 104*, 4559–4570.
London, R. E. (1980) in *Magnetic Resonance in Biology* (Cohen, J. S., Ed.) pp 1–69, Wiley, New York.
Marion, D., Ikura, M., & Bax, A. (1989) *J. Magn. Reson. 84*, 425–430.
Meiboom, S., & Gill, D. (1958) *Rev. Sci. Instrum. 29*, 688–691.
Messerle, B. A., Wider, G., Otting, G., Weber, C., & Wüthrich, K. (1989) *J. Magn. Reson. 85*, 608–613.
Modrich, P., & Richardson, C. C. (1976) *Proc. Natl. Acad. Sci. U.S.A. 73*, 780–784.
Nicholson, L. K., Kay, L. E., Baldisseri, D. M., Arango, J., Young, P. E., Bax, A., & Torchia, D. A. (1992) *Biochemistry 31*, 5253–5263.
Nirmala, N. R., & Wagner, G. (1988) *J. Am. Chem. Soc. 110*, 7557–7558.
O'Donnell, T. J., & Olson, A. J. (1981) *Comput. Graphics 15*, 133–142.
Palmer, A. G., III, Rance, M., & Wright, P. E. (1991a) *J. Am. Chem. Soc. 113*, 4371–4380.
Palmer, A. G., III, Cavanagh, J., Wright, P. E., & Rance, M. (1991b) *J. Magn. Reson. 93*, 151–170.
Palmer, A. G., III, Skelton, N. J., Chazin, W. J., Wright, P. E., & Rance, M. (1992) *Mol. Phys. 75*, 699–711.
Press, W. H., Flannery, B. P., Teukolsky, & Vetterlimg, W. T. (1986) *Numerical Recipes*, Cambridge University Press, Cambridge.
Ratkowsky, D. (1983) *Nonlinear Regression Modeling*, Marcel Dekker, New York.
Richardson, J. S. (1981) *Adv. Protein Chem. 34*, 167–339.
Russel, M., & Model, P. (1985) *Proc. Natl. Acad. Sci. U.S.A. 82*, 29–33.
Russel, M., & Model, P. (1986) *J. Biol. Chem. 261*, 14997–15005.
Schneider, D. M., Dellwo, M. J., & Wand, A. J. (1992) *Biochemistry 31*, 3645–3652.
Shoji, A., Ozaki, T., Fujito, T., Deguchi, K., Ando, S., & Ando, I. (1989) *Macromolecules 22*, 2860–2863.
Smith, G. P., Yu, L. P., & Domingues, D. J. (1987) *Biochemistry 26*, 2202–2207.
Söderberg, B.-O., Sjöberg, B.-H., Sonnerstam, U., & Brändén, C.-I. (1978) *Proc. Natl. Acad. Sci. U.S.A. 75*, 5827–5830.
Stone, M. J., Fairbrother, W. J., Palmer, A. G., III, Reizer, J., Saier, M. H., Jr., & Wright, P. E. (1992) *Biochemistry 31*, 4394–4406.
Vold, R. R., & Vold, R. L. (1976) *J. Chem. Phys. 64*, 320–332.
Wright, L. L., Palmer, A. G., III, & Thompson, N. L. (1988) *Biophys. J. 54*, 463–470.
Zang, L., Laughlin, M. R., Rothman, D. L., & Shulman, R. G. (1990) *Biochemistry 29*, 6815–6820.